Experimental phase synchronization detection in non-phase coherent chaotic systems by using the discrete complex wavelet approach

Maria Teodora Ferreira, Rosangela Follmann, Margarete O. Domingues, Elbert E. N. Macau, and István Z. Kiss

Citation: Chaos **27**, 083122 (2017); doi: 10.1063/1.4999908
View online: http://dx.doi.org/10.1063/1.4999908
View Table of Contents: http://aip.scitation.org/toc/cha/27/8
Published by the American Institute of Physics

Experimental phase synchronization detection in non-phase coherent chaotic systems by using the discrete complex wavelet approach

Maria Teodora Ferreira,[1,a)] Rosangela Follmann,[1,b)] Margarete O. Domingues,[1,c)] Elbert E. N. Macau,[1,d)] and István Z. Kiss[2,e)]
[1]*Associated Laboratory for Computing and Applied Mathematics (LAC), Brazilian National Institute for Space Research (INPE), São José dos Campos 12227-010, Brazil*
[2]*Department of Chemistry, Saint Louis University, St. Louis, Missouri 63103, USA*

(Received 12 March 2017; accepted 11 August 2017; published online 28 August 2017; corrected 30 August 2017)

Phase synchronization may emerge from mutually interacting non-linear oscillators, even under weak coupling, when phase differences are bounded, while amplitudes remain uncorrelated. However, the detection of this phenomenon can be a challenging problem to tackle. In this work, we apply the Discrete Complex Wavelet Approach (DCWA) for phase assignment, considering signals from coupled chaotic systems and experimental data. The DCWA is based on the Dual-Tree Complex Wavelet Transform (DT–CWT), which is a discrete transformation. Due to its multi-scale properties in the context of phase characterization, it is possible to obtain very good results from scalar time series, even with non-phase-coherent chaotic systems without state space reconstruction or pre-processing. The method correctly predicts the phase synchronization for a chemical experiment with three locally coupled, non-phase-coherent chaotic processes. The impact of different time-scales is demonstrated on the synchronization process that outlines the advantages of DCWA for analysis of experimental data. *Published by AIP Publishing.*
[http://dx.doi.org/10.1063/1.4999908]

Several types of synchronization have been described theoretically and observed experimentally. Among them, the most prominent are complete synchronization, lag synchronization, and generalized synchronization.[1] Our focus in this article is the detection of phase synchronization between two systems, where a certain relation between phases appears, while their amplitudes can remain without significant correlation.[2–6] We are particularly interested here in situations in which we have a scalar data set to analyse, which is often the case with experimental measurements.

I. INTRODUCTION

The phenomenon of synchronization has been extensively reported in natural systems, such as in heart cells, applause, flashing of the South-East Asian fireflies, and chirping of crickets.[7–11] Historically, synchronization is understood as a mutual rhythm adjustment of periodic oscillators, due to some type of interaction between them.[1] Considerable progress has been made towards precisely generalizing the concept of synchronization, allowing the concept to encompass chaotic oscillators.[1,3–6,12–16] Several types of synchronization have been described theoretically and observed experimentally. Among them, the most prominent are complete synchronization, lag synchronization, and generalized synchronization.[1]

Our focus in this article is the detection of phase synchronization between two systems, where a certain relation between phases appears, while their amplitudes can remain without significant correlation.[2–6] We are particularly interested here in situations in which we have a scalar data set to analyse, which is often the case with experimental measurements. Therefore, investigating phase synchronization requires a well-defined phase assignment out of the scalar data series, in order to test the condition $\Delta\phi(t) = |\phi_2(t) - \phi_1(t)| < cons\tan t$, where $\phi_1(t)$ and $\phi_2(t)$ are the phases of two systems. To assign such phase variables using a scalar data series, many methods require, directly or indirectly, state space reconstruction. After that, one can use direct measurements of the phase angle on a projection of the attractor, as well as more sophisticated techniques such as: measurement on a proper Poincaré surface of section, curvature and recurrence plots,[17,18] or localized sets.[19] The methods that can be applied straightforwardly to scalar data series include phase estimation by means of frequency method,[20,21] synchrosqueezed wavelet transforms,[22] protophases,[23] Hilbert transform,[3,24] and the continuous complex wavelet transform.[25–35]

The methods lead to consistent results when the underlying system is a phase coherent one, i.e., it is possible to find an appropriate projection so that the system trajectory circles around a rotation center. However, this is not the case for non-phase coherent systems,[1] which generate broad-band spectrum signals. For these systems, with certain limitations, scalar data series can be used to obtain the phase with the Hilbert transform[3,24] by searching for a unique center of

[a)]Electronic mail: mteodoraf25@gmail.com
[b)]Electronic mail: rosangelafollmann@gmail.com
[c)]Electronic mail: margarete.domingues@inpe.br
[d)]Electronic mail: elbert.macau@inpe.br
[e)]Electronic mail: izkiss@slu.edu

rotation of the trajectories in the signal vs Hilbert transform state space. Nevertheless, there are cases for which the Hilbert transform is not able to keep track of fast transitory phase changes of the system,[20,21] leading to artifacts. To address this drawback, a methodology based on a continuous complex wavelet transform that uses the complex Morlet wavelet to obtain the phase of scalar chaotic time series was introduced.[30,36] In fact, this method is considered as one of the most effective approaches for reconstruction of the phase of the signal.[37,38]

The methodology, however, has a high computational cost and may present some difficulties to analyse the results due to its redundancy framework when applied to large time series. Additionally, the method involves selection of method parameters that are sometime difficult to obtain.[37,38]

To overcome these difficulties, we proposed an approach, namely, Discrete Complex Wavelet Approach (DCWA)[39] for phase assignment. This approach is based on the Dual-Tree Complex Wavelet Transform (DT–CWT) and was introduced for phase assignment to non-linear oscillators. The applicability of our DCWA has been verified in chaotic Rössler systems in phase-coherent and non-phase-coherent regimes,[40,41] chaotic Lorenz systems,[42,43] and Kuramoto Model with different settings.[44]

In this paper, we show that, through application to the synchronization in a complex chaotic chemical process, DCWA is a very efficient method for phase synchronization detection. We demonstrate how to detect phase synchronization among three locally coupled chaotic electrochemical oscillators for which the determination of phase synchronization phenomenon presents considerable intrinsic difficulties. We explore the implementation through a computationally efficient means that allows an accurate characterization of the phase synchronization phenomena. The remainder of this paper is organized as follows. In Sec. II, we present the DCWA, the arctangent method, and Hilbert Transform. Then, in Sec. III, the results and analysis of the chaotic systems and experimental data are presented, and in Sec. IV, we provide the conclusion.

II. METHODS

In this section, we describe how to calculate the phase using DCWA. (Further details are given in a previous publication.[39]) For comparison, we also describe the arctangent method (Subsection II B) and Hilbert Transform (Subsection II C).

A. Discrete complex wavelet approach (DCWA): Energy and phase computation

In order to calculate the phase of a chaotic system using the DCWA, the time series of a scalar variable x of the system is analyzed by the multi-scale Dual-Tree Complex Wavelet Transform (DT–CWT), according to the scheme in Fig. 1(a). For details on the DT–CWT, see Appendix A and Ref. 45. As the output of this transformation, we have the time series of the complex wavelet coefficients $\boldsymbol{d}^j$ at each scale j. With these coefficients, the energy E^j at each scale j is calculated as the square of the modulus of complex wavelet coefficients, i.e., $E^j(n) = |\boldsymbol{d}^j(n)|^2$. After that, the *global wavelet spectrum* is computed as follows:

$$\mathbb{E}^j = \sum_n E^j(n). \tag{1}$$

In the next step, we take the scale J in which the global wavelet spectrum energy is the maximal, i.e., $\mathbb{E}^J = \max_j \mathbb{E}^j$. The maximum energy considering all the scales obtained by the global wavelet spectrum are the natural candidates to be used for calculating the phase. Among them, in general, we discard scales which have an insufficient number of points to represent the phase time series correctly. This is due to the fact that as the scales have an insufficient number of points, they cannot identify the localized structures in the case of the discrete wavelet. Finally, the selected scale J is used to extract the phase time series $\phi^J(t) = a\tan 2(\underline{d}^J, \bar{d}^J)$. The atan2 is the arctangent function with two arguments: $\underline{d}^j$ is the imaginary part of the complex wavelet coefficient in the scale J and $\bar{d}^J$ is the real part of the complex wavelet coefficient in the scale J.

Consider now two systems with time series x_1 and x_2. The method described above applied to both of them can be viewed in Fig. 1(b). When J_1 was different from J_2, we chose the scale $J = \min(J_1, J_2)$. This choice was based on the fact that the number of points N in this multi-scale phase time series is proportional to the scale, i.e., $N = 2^{L=J}$; therefore, we chose the larger phase time series. Subsequently, the phase time series of each system, ϕ_1^J and ϕ_2^J, are straightforwardly calculated. The instantaneous

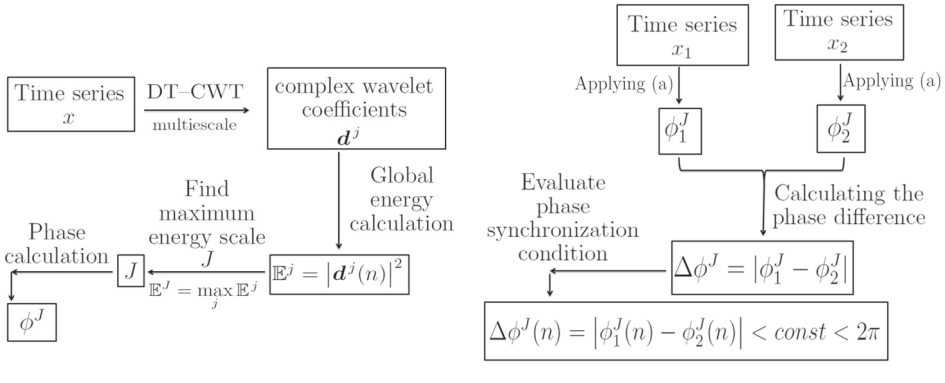

FIG. 1. Schematic representation the DCWA. In inset (a), a single time series x is considered. Inset (b) illustrates the application of the DCWA in two series, x_1 and x_2.

phase difference between the systems is computed as $\Delta\phi^J_{12} = |\phi^J_2 - \phi^J_1|$, which allows one to check for the phase synchronization condition $\Delta\phi^J_{12} = |\phi^J_2 - \phi^J_1| < constant$. The DCWA method is schematically represented in Fig. 1.

B. Arctangent method

The Arctangent method is the most common method for measuring phase when it is possible to project the underlying attractor on a plane so that the projection is a smeared limit cycle[12] with well-defined rotation center.

In this and other similar cases, the phase $\phi(t)$ presents a coherent phase and it can be measured as the angle in the polar coordinate system on the plane (x, y), as proposed by Rosenblum *et al*. in Ref. 3, as follows:

$$\phi(t) = \tan^{-1}\left(\frac{y}{x}\right). \tag{2}$$

When the system displays a non-coherent oscillation, the phase can be defined by using the projection of the attractor on the plane of the derivative, as proposed in Ref. 46 by using the equation

$$\phi(t) = \tan^{-1}\left(\frac{\dot{y}}{\dot{x}}\right). \tag{3}$$

Note that to calculate the phase by using these methods, it is necessary to know the two state variables, namely, x and y, which is not always available.

In this approach, the arctangent function is defined as a four-quadrant operation.

C. Hilbert transform

A consistent way to define the phase for an arbitrary signal is known in signal processing as the analytic signal concept, as can be seen in Ref. 1. This general approach, based on the Hilbert transform (HT), unambiguously gives the instantaneous phase $\phi(t)$ and amplitude $A(t)$ for a signal $s(t)$ via construction of the analytic signal $\zeta(t)$, which is a complex function of time defined as (Ref. 1)

$$\zeta(t) = s(t) + \imath\, s_H(t) = A(t)\, e^{\imath\phi(t)}. \tag{4}$$

Here, the function $s_H(t)$ is the HT of $s(t)$

$$s_H(t) = \pi^{-1}\, P.V. \int_{-\infty}^{\infty} \frac{s(\tau)}{t-\tau} d\tau, \tag{5}$$

where P.V. means that the integral is taken in the sense of the Cauchy principal value.

In Sec. III, we describe the chaotic systems and experimental data, as well as the results obtained from the applicability the DCWA.

III. RESULTS

In this section, we present the phase synchronization analysis of the simulated data from Rössler systems and then of experimental data.

A. Simulated data

To demonstrate the definition of phase, we first consider uncoupled Rössler systems, both in phase-coherent and non-phase-coherent regimes. Then, we analyze the effects of coupling on systems in both regimes. The time series is obtained from two non-identical Rössler systems,[47] using a Runge-Kutta 4th order method with an integration time step of 0.01. In order to verify the applicability of the DCWA in time series with large numbers of points, $N = 2^{23}$ number of points are also used. For each Rössler system, we study the use of x and y time series to test the method for the choice of observable variables. The DCWA is applied considering $j = 17$ scales of decomposition. From this decomposition scale, it is possible to obtain the reconstruction of wavelet and avoid edge effects.

1. Uncoupled Rössler system

The uncoupled Rössler system used in the tests is described by

$$\begin{aligned} \dot{x} &= -y - z, \\ \dot{y} &= x + ay, \\ \dot{z} &= 0.4 + z(x - 8.5), \end{aligned} \tag{6}$$

where the parameter a sets the attractor dynamics to be in phase-coherent or non-phase-coherent regime.

Figure 2(a) shows the projection of the attractor of the Rössler system in phase-coherent regime with $a = 0.16$. The non-phase-coherent Rössler attractor with $a = 0.2925$ is shown in Fig. 2(b). The corresponding global wavelet spectrum obtained using the x and y variables (denoted by E_x and E_y, respectively) are depicted in Figs. 2(c) and 2(d), considering phase-coherent and non-phase-coherent regimes, respectively. Note from the global wavelet spectrum that the maximum energy scale for both cases, x or y variables, is $J = 9$. Therefore, this scale was applied to obtain the phase in both cases. The phase obtained using the x and y variables in the scale $J = 9$ is denoted by $\phi_x^{J=9}$ and $\phi_y^{J=9}$, respectively. Note that the phases grow practically uniform as expected for a phase-coherent regime, which can be seen in Fig. 2(e). The small deviations can occur due to the different periods of the unstable periodic orbits that the trajectory intermittently approaches. For the system in the non-phase-coherent regime, these deviations are larger, as expected [see Fig. 2(f)].

2. Rössler system in phase-coherent regime

Let us consider now two Rössler systems, in a phase-coherent regime coupled bidirectionally by variable y, described by the following equations:

$$\begin{aligned} \dot{x}_{1,2} &= -\omega_{1,2}\, y_{1,2} - z_{1,2}, \\ \dot{y}_{1,2} &= \omega_{1,2}\, x_{1,2} + 0.16\, y_{1,2} + \eta\,(y_{2,1} - y_{1,2}) \\ \dot{z}_{1,2} &= 0.4 + z_{1,2}\,(x_{1,2} - 8.5), \end{aligned} \tag{7}$$

in which $\omega_1 = 0.98$ and $\omega_2 = 1.02$ define the mismatch in the natural frequencies and parameter η is the intensity of coupling between these two systems.

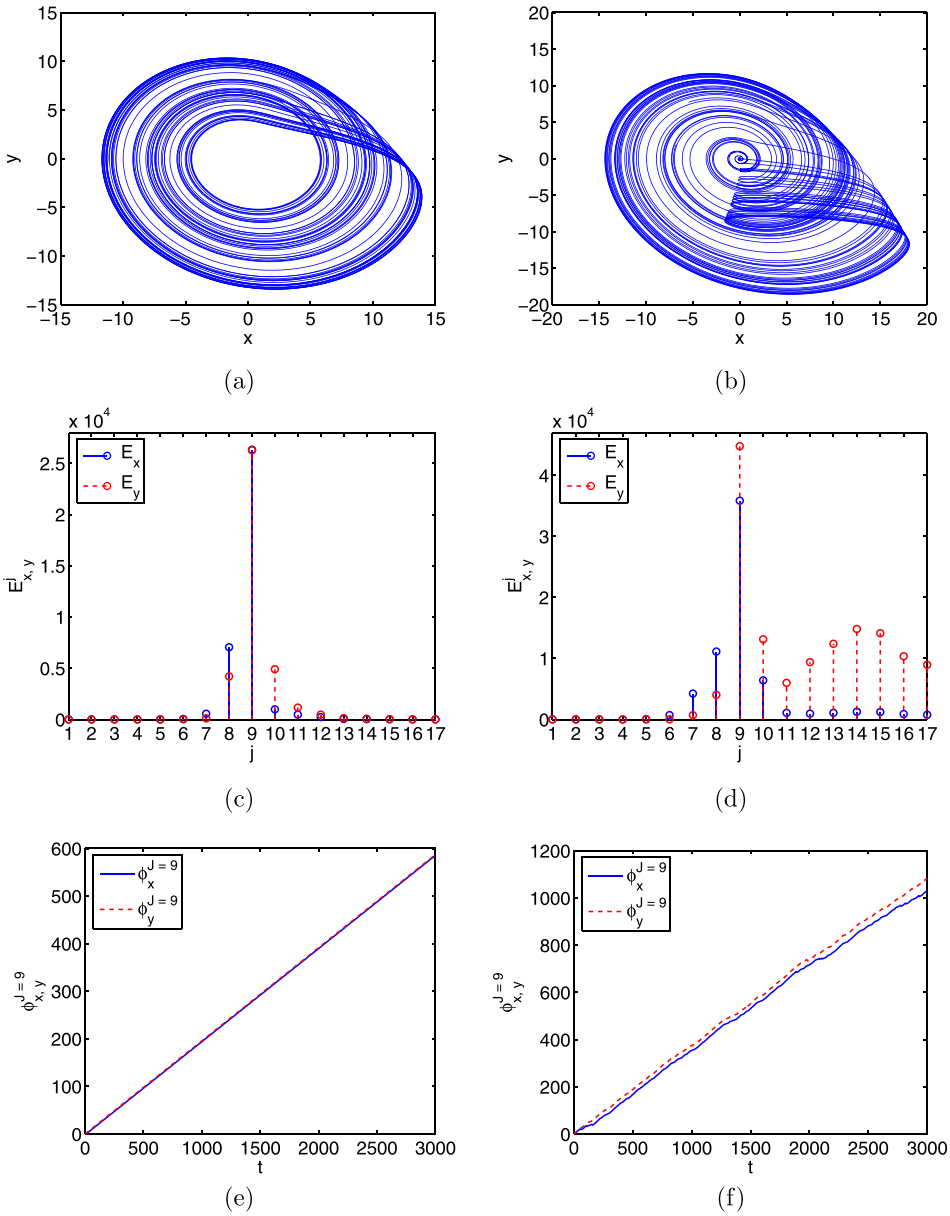

FIG. 2. (a) and (b), The projection of the attractor of the Rössler system considering a phase-coherent regime, $a = 0.16$ and a non-phase-coherent regime, $a = 0.2925$, respectively. The global wavelet spectrum in (c) phase-coherent and (d) non-phase-coherent regimes. The phase in (e) phase-coherent and (f) non-phase-coherent regimes.

In this application, three different intensities of coupling were considered: very weak, medium, and strong. The coupling strengths were empirically adjusted to obtain three possible states for the analysis of the systems: not phase synchronized, phase-slips, and in-phase synchronization.

For different coupling intensities η, we compared the DCWA with the arctangent method.

According to the analysis, we observe from the global wavelet spectrum that the maximum energy scale for both cases, by using x or y variables, is $J = 9$. Thus, the phase was calculated considering this scale.

The phase difference between these systems is shown in Fig. 3; in (a) using the DCWA and in (b) comparing the DCWA and the arctangent method considering $\eta = 0.035$.

In Fig. 3(a), $|\Delta\phi_x^{J=9}|$ denotes the phase difference calculated with DCWA considering the scale $J = 9$ and using the x variable. In Fig. 3(b), $\Delta\phi_x^{DCWA}$ and $\Delta\phi_y^{DCWA}$ denote the phase difference calculated by applying the DCWA, considering the scale $J = 9$ and using the x and y variables, respectively. The outcome of the arctangent method is denoted by $\Delta\phi^{arctangent}$.

For the three intensities of coupling studied, the DCWA presents similar results to the arctangent method. For small intensity of coupling $\eta = 0.01$, the phase difference increases with time, which characterizes the absence of phase synchronization. If the coupling strength is increased to $\eta = 0.035$, some phase-slips appear. Note in Fig. 3(b) that phase-slips are detected for both methods. In Fig. 3(c), the interval $t = [1300, 1400]$ of the original time series is shown to illustrate the phase-slips. When $\eta = 0.05$, phase synchronization sets in.

3. Rössler system in non-phase-coherent regime

We include here the results related to two Rössler systems in a non-phase-coherent regime, coupled bidirectionally through variable x. The system is given by Eq. (8) and the parameters considered are based on the studies in Refs. 1 and 21

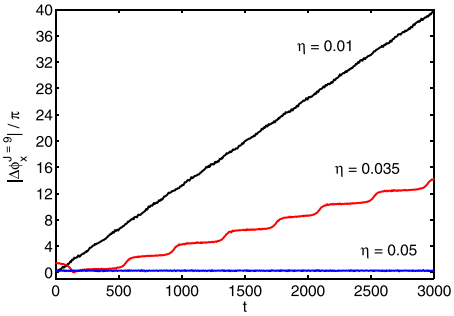

(a)

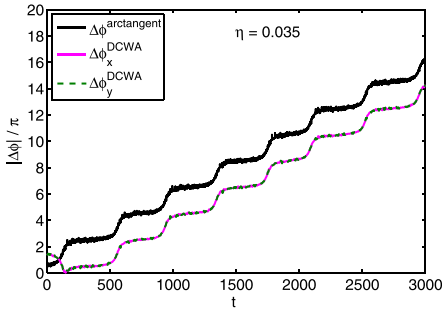

(b)

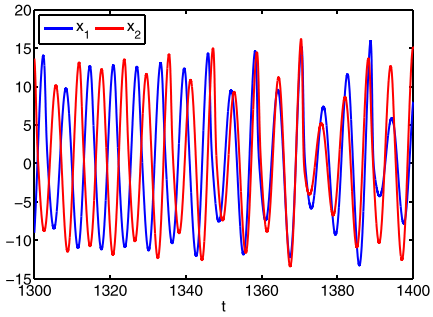

(c)

FIG. 3. Phase differences between two Rössler systems coupled bidirectionally by variable y considering phase-coherent regime and applying in (a) the DCWA and (b) the DCWA compared with the arctangent method, considering $\eta = 0.035$. (c) The interval $t = [1300, 1400]$ of the original time series where phase-slips occur.

$$\begin{aligned}\dot{x}_{1,2} &= -\omega_{1,2}\, y_{1,2} - z_{1,2} + \eta\,(x_{2,1} - x_{1,2}),\\ \dot{y}_{1,2} &= \omega_{1,2}\, x_{1,2} + 0.2925\, y_{1,2},\\ \dot{z}_{1,2} &= 0.4 + z_{1,2}\,(x_{1,2} - 8.5),\end{aligned} \tag{8}$$

where $\omega_1 = 0.98$ and $\omega_2 = 1.02$.

In this application, two different intensities of coupling were considered: very weak and strong. According to the analysis, we observe from the global wavelet spectrum that the maximum energy scale for both cases, by using x or y variables, is $J = 9$ and the phase was calculated considering this scale.

The phase difference between the two systems using the DCWA is shown in Figs. 4(a) and 4(b), denoted by $|\Delta\phi_x^{J=9}|$ and $|\Delta\phi_y^{J=9}|$, using the x and y variables of the time series, respectively. Note in Fig. 4 that for small coupling intensity $\eta = 0.05$, the phase difference increases with time, characteristic of systems that are not phase-synchronized. When $\eta = 0.2$, phase synchronization occurs.

4. Rössler systems with noise

The robustness of the DCWA is investigated with the addition of Gaussian noises to the x_1, x_2, y_1, y_2 components of the two Rössler system in non-phase-coherent regime ($a = 0.2925$), according to the following equations:

$$\begin{aligned}\dot{x}_{1,2} &= -\omega_{1,2} y_{1,2} - z_{1,2},\\ \dot{y}_{1,2} &= \omega_{1,2} x_{1,2} + a y_{1,2} + \eta(y_{2,1} - y_{1,2}),\\ \dot{z}_{1,2} &= 0.4 + z_{1,2}(x_{1,2} - 8.5),\end{aligned} \tag{9}$$

where $\omega_1 = 0.98$ and $\omega_2 = 1.02$.

The coupling intensity $\eta = 0.30$ is considered in order to analyze the phase synchronization between the two systems.

The noise is added to the temporal series, for example, x_1, as follows:

$$rx1 = \alpha \cdot std(x_1)) \cdot (randn(length(x_1), 1))$$

in which α is the percentage of noise added the time series; $std(x_1)$ is the standard deviation of the elements of x_1; *randn* creates a matrix with underlying class of double, with Normally distributed random numbers in all elements. After generated, the noise is added to the respective temporal series in question.

In the DCWA, in all cases, the maximum energy scale is $J = 9$. Therefore, the phase is calculated considering this

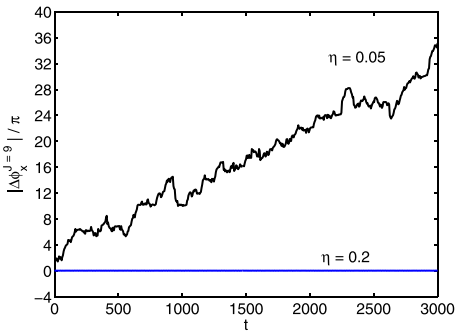

(a)

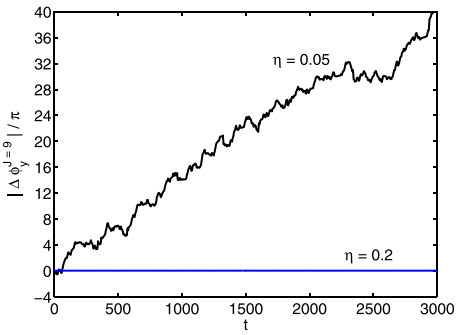

(b)

FIG. 4. Phase differences between two Rössler systems coupled bidirectionally by variable x considering non-phase-coherent regime and applying the DCWA using in (a) the x variable of the time series and (b) the y variable of the time series.

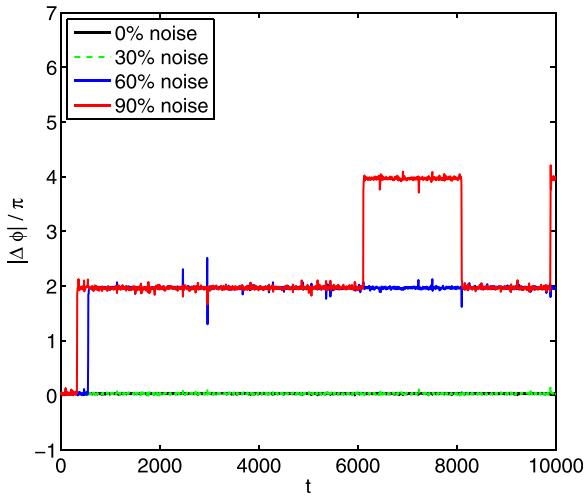

FIG. 5. Phase differences between two coupled Rössler systems in non-phase-coherent regime with $\eta = 0.30$ and considering 0%, 30%, 60%, and 90% of noise.

scale. Figure 5 shows the phase difference between two coupled chaotic Rössler systems in non-phase-coherent, considering 0%, 30%, 60% and 90% noise.

The results indicate the robustness of the DCWA considering low levels of noise. When we consider the Rössler system in non-phase-coherent regime, the DCWA allows to identify that, with 0% and 30% noise, correctly, the two systems are synchronized in phase (see Fig. 5). We emphasize that the method is able to work properly with experimental even in the presence of middle level of noise.

B. Experimental data

In this section, we apply DCWA for characterization of the phase dynamics of electrochemical oscillations that take place in a system of three locally coupled electrodes, as can be seen in Ref. 48.

The experimental setup consists of three nickel wires applied as the working, and a Pt wire as the counter electrode in an electrochemical cell. A potentiostat sets a constant potential that drives the reaction such that the potential difference constant between the wires and a Hg/Hg_2SO_4/saturated K_2SO_4 reference electrode. The current, proportional to the rate of metal dissolution on each wire, is measured; this data will be used for time series analysis. A schematic of the experimental setup is shown in Fig. 6(a).

Two identical coupling resistances R were introduced between the Ni electrodes to induce local interactions between electrodes x, y, and z as shown in Fig. 6(a); the schematic of locally coupled configuration is shown in Fig. 6(b). Further details about the experiments are given in a previous publication.[48]

We analysed two data sets, composed of $N = 200$ and 500 points and classified as set *I*: having three weakly coupled oscillators and set *II*: having three strongly coupled oscillators. The same data set was analysed previously in Ref. 49; because reconstruction of phase variables of the non-phase-coherent chaotic signal was problematic, in the previous work, a recurrence-plot based method was applied to identify the network topology of the system. Here, we focus on applying DCWA to characterize the phase dynamics of the system.

Figures 6(c) and (d) show a time window for the data series of the oscillators x, y, and z of the set I and set II, respectively. The results obtained from the DCWA are compared with the application of Hilbert transform; see Subsection II C for details in the Hilbert transform. The phase differences calculated via Hilbert transform considering the oscillators x and y are denoted by $\Delta\phi_{xy}^{Hilbert}$; between

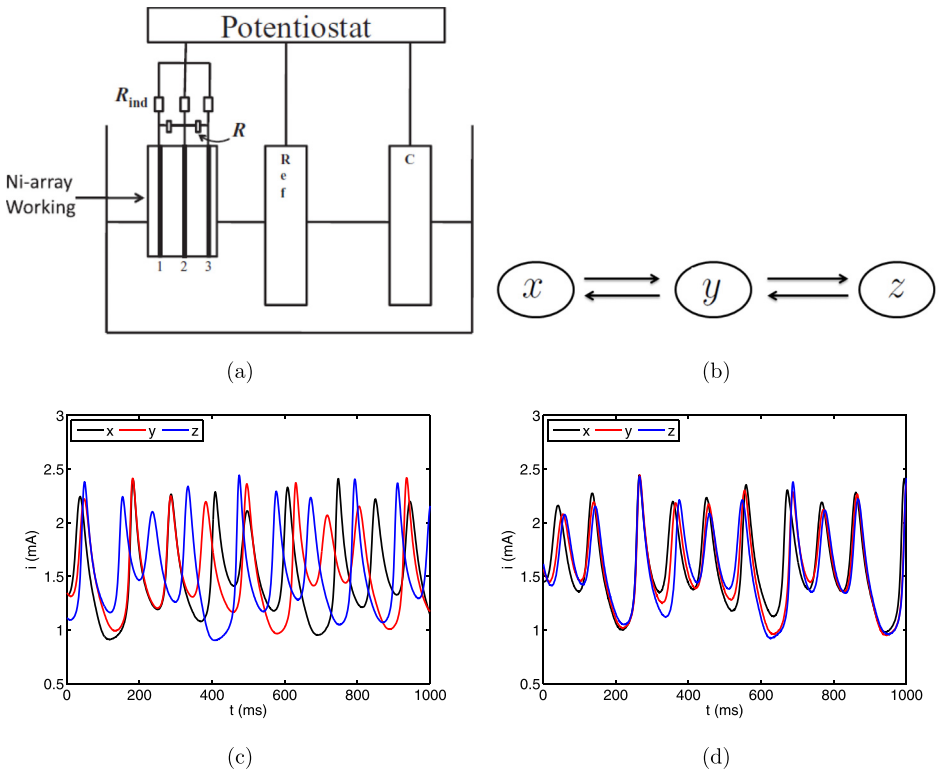

FIG. 6. Experimental setup, for details, see Ref. 48. (a) Diagram of the electrochemical cell; (b) topology of the coupling of the three oscillators; (c) an interval of time series of oscillators x, y, and z of the set I;and (d) an interval of time series of oscillators x, y, and z of the set II.

oscillators x and z are $\Delta\phi_{xz}^{Hilbert}$ and between oscillators y and z are $\Delta\phi_{yz}^{Hilbert}$.

Figure 7 illustrates the results obtained from the analysis of the set I showing (a) global wavelet spectrum and (b)–(d) the phase difference in the time interval $t = [0, 100\text{s}]$ considering (b) DCWA with the scale $J = 6$; (c) DCWA with the scale $J = 7$; and (d) the Hilbert transform.

We can observe in Fig. 7(a) that for the three oscillators the scale of the maximum energy is $J = 7$. For comparison, in addition to the phase corresponding to $J = 7$ [Fig. 7(b)], we also calculated the phase corresponding to $J = 6$ [Fig. 7(c)]. This latter phase describes the behavior at faster timescales. While scale $J = 8$ also has comparable energies to scales $J = 6$ and 7, the phase of this slow scale was not considered because of the insufficient number of points to well represent the phase of the time series. In addition, this scale would represent the behavior of slow drift in the time series due to small changes in surface conditions during the chemical reactions. According to the phase differences illustrated in Figs. 7(b) and 7(c), we can confer that the phase differences between the oscillators diverge in a complex manner, i.e., the system is not phase synchronized. The Hilbert transform based phase differences are also not bounded; however, note that the phase differences in Fig. 7(d) reach very large values (e.g., 1200 rad); this value is not consistent with the slightly dissimilar nature of the oscillators and due to the lack of center of rotation in the two-dimensional projection with the Hilbert transform.

Figure 8 illustrates the results obtained from the analysis of the set II showing the (a) global wavelet spectrum and (b)–(d) the phase difference in the time interval $t = [0, 100\text{s}]$ considering (b) DCWA by using the scale $J = 6$; (c) DCWA by using the scale $J = 7$; and (d) the Hilbert transform.

We can observe in Fig. 8(a) that for the three oscillators the scale of the maximum energy is again for the scale $J = 7$. (Similarly, for the weak coupling case, we also show results for the fast $J = 6$ scale.) Based on the phase difference $J = 6$ [Fig. 8(b)], the three oscillators are almost perfectly phase locked. For scale $J = 7$ [Fig. 8(c)], there are some variations of the phase difference over time; however, we see that for the time series data of about 500 cycles, the overall phase differences are less than 4π radians, indicating the presence of bounded phase difference and strong phase synchronization. We also see that due to the non-phase-coherent character, even for this relatively strong coupling, the oscillations do not simply phase-lock, but instead there is a complex phase-difference dynamics with bounded phase difference. With respect to the results obtained using the Hilbert transform, as can be seen in Fig. 8(d), the phase difference exhibits diverging trend, again because of the lack of center of rotation in the 2D projection, making it impossible to properly infer that the oscillators are synchronized in phase.

The impact of slow $J = 7$ and fast $J = 6$ scales on the dynamics can be also seen in the variation of energy of the corresponding scales shown in Fig. 9. The energy of the slow scale $J = 7$ variation exhibits sporadic spikes compared

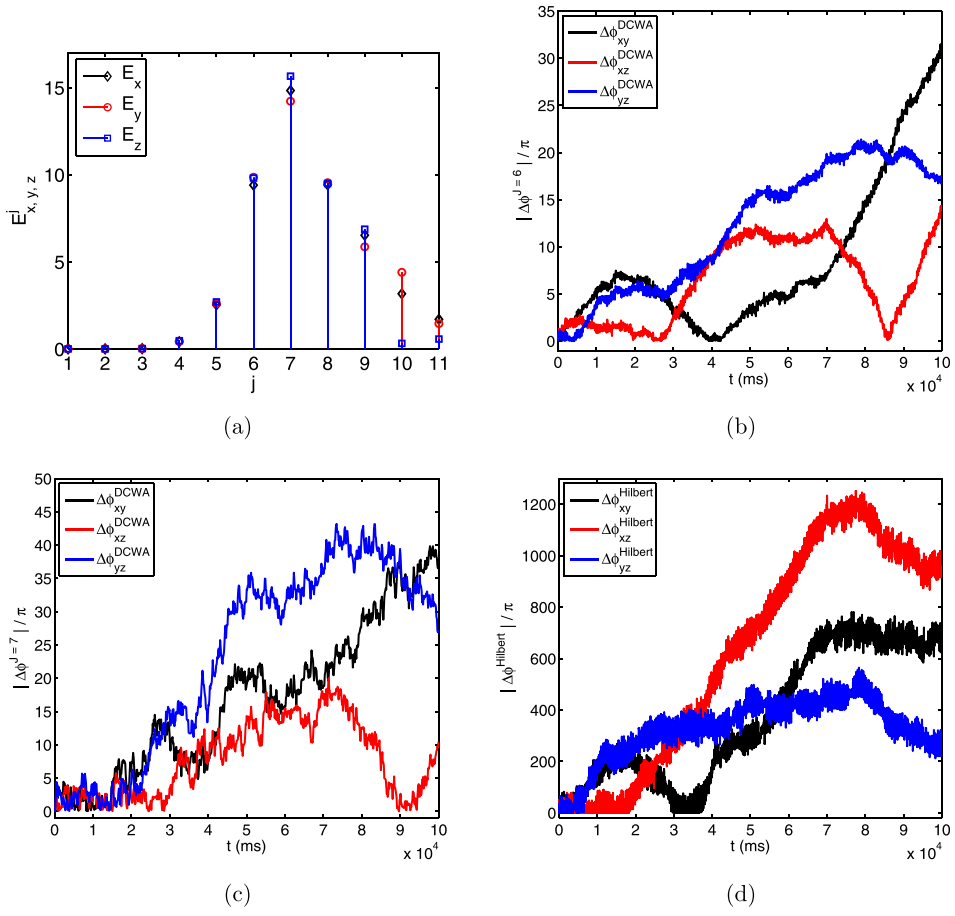

FIG. 7. The results obtained from the analysis of the set I showing in (a) global wavelet spectrum and (b)–(d) the phase difference in the time interval $t = [0, 100\text{s}]$ considering (b) the DCWA by using the scale $J = 6$; (c) the DCWA by using the scale $J = 7$; and (d) the Hilbert transform.

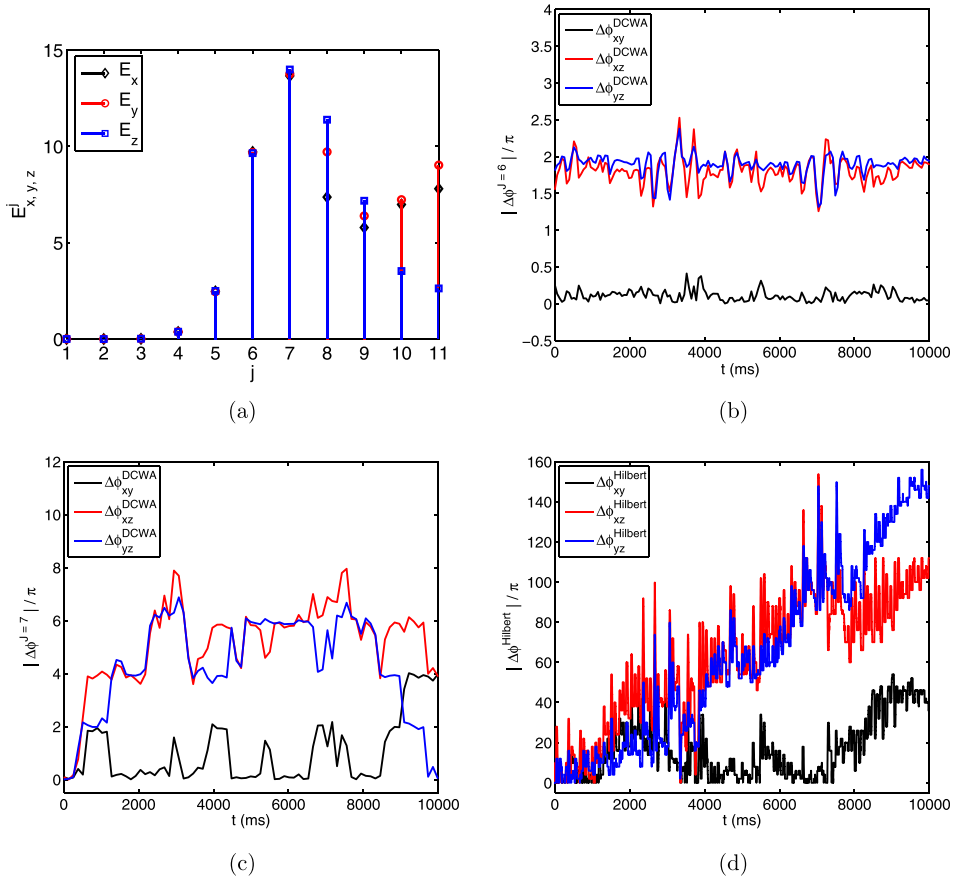

FIG. 8. The results obtained from the analysis of the set *II* showing in (a) global wavelet spectrum and (b)–(d) the phase difference in the time interval $t = [0, 100\text{s}]$ considering (b) the DCWA by using the scale $J = 6$; (c) the DCWA by using the scale $J = 7$; and (d) the Hilbert transform.

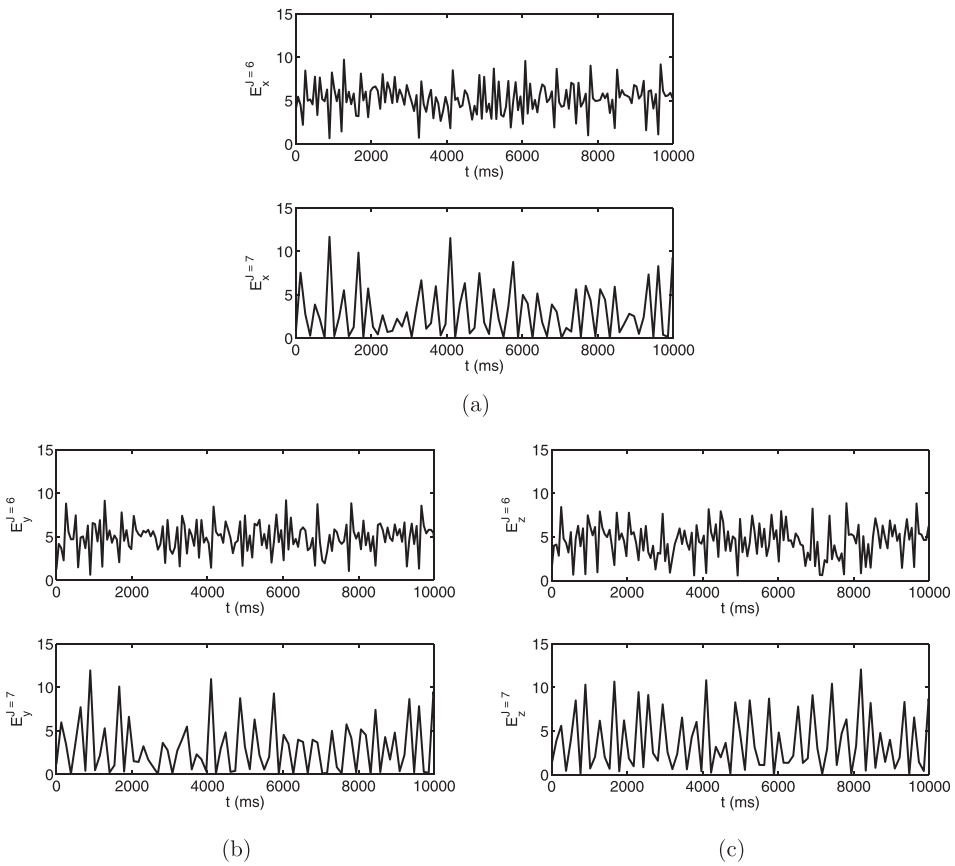

FIG. 9. The results obtained from the analysis of the set *II* showing the energy time series in the time interval $t = [0, 10\text{s}]$, in the scale $J = 6$ and $J = 7$ for the three oscillators, considering oscillators x (a), y (b), and z (c).

with the relatively constant energy of the fast scale $J=6$. While for most time intervals, $J=6$ scale dominates the system, intermittently, when the corresponding energy is large, $J=7$ scales should be considered as well. We note that such time-scale separation did not impact the final conclusion about phase synchronization in the given system, but it is certainly possible that careful choice of the scale must be made in systems with largely varying time-scales.

The lack of phase synchronization for set *I* and the presence of phase synchronization in set *II* are consistent with the previous result obtained with the recurrence plot method.[49] We note that with DCWA, the result was obtained without state space reconstruction in a computationally effective method using discrete wavelets.

IV. CONCLUSION

In this paper, we evaluated the applicability of the Discrete Complex Wavelet Approach—DCWA for phase assignment to chaotic systems and experimental data. The performance of the DCWA in comparison with other known methods was verified based on the results obtained to detect phase synchronization between two coupled Rössler systems in both phase-coherent and non-phase-coherent regimes. The DCWA correctly detects phase synchronization in two coupled chaotic Rössler systems in both phase-coherent and non-phase-coherent regimes. Regarding the results from the analysis of electrochemical oscillators, DCWA was able to correctly verify the phase synchronization of the oscillations; the presence of non-phase coherence was effectively handled by the algorithm by time-scale separation of the different processes. In particular, DCWA requires only a scalar time series of the system without the need of reconstruction of the attractor, a very convenient feature, especially in the case of experimental data.

ACKNOWLEDGMENTS

This work was supported by CAPES, CNPq (Grant Nos. 306038/2015-3, 309667/2013-5, 306828/2010-3, 304582/2010-7, 483226/2011-4, and 10571/13-2) and FAPESP (Grant Nos. 2015/25624-2 and 2015/50122-0). I.Z.K. acknowledges support from National Science Foundation (CHE-1465013 grant) and Professor N. Kingsbury for the DT-CWT algorithm and scientific discussions.

Research supported by Grant Nos. 2015/50122-0 Sao Paulo Research Foundation (FAPESP) and DFG-IRTG 1740/2.

APPENDIX A: DUAL-TREE COMPLEX WAVELET TRANSFORM

The DT–CWT is a well crafted transform, from a mathematical and filter bank theory point of view, introduced by Kingsbury in the late 1990s, as can be seen in Refs. 45 and 50–53.

In practice, DT–CWT employs two real Discrete Wavelet Transform (DWT); for more details about the DWT, see in Refs. 54 and 55. A schematic representation of the DT–CWT decomposition is illustrated in Fig. 10. Herein, the notation overline and underline are used to identify the upper and lower decomposition tree filters, functions, and

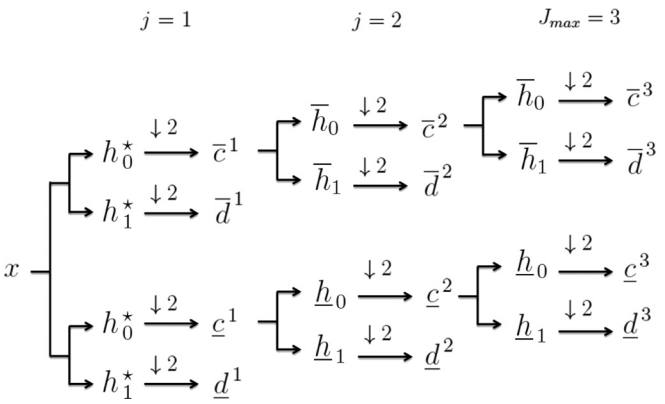

FIG. 10. Schematic multi-scale representation of three scales DT–CWT decomposition of the real time series x in three levels, where the filters $h_0^\star$ and $h_1^\star$ are considered in the level $j=1$. In levels $j=2$ and $j=3$, the filters of the upper and lower tree are $\bar{h}_0$, $\bar{h}_1$ and $\underline{h}_0$, $\underline{h}_1$, respectively.

coefficients, while the boldface is used to identify the complex functions and coefficients. The real time series x is decomposed in scales $j=1,\ldots,J_{max}$, and the notation * is included in the first scale filters, $h_0^\star$ and $h_1^\star$. The first DWT is associated with a filter bank of the upper tree, and it uses low-pass filters $\bar{h}_0$ and high-pass filters $\bar{h}_1$. It computes the multilevel real wavelet coefficients $\bar{d}^j$ that will be used as the real part of the desired complex wavelet coefficients $\boldsymbol{d}^j$. The second DWT is associated with a filter bank of the lower tree, and it is composed of low-pass filters $\underline{h}_0$ and high-pass filters $\underline{h}_1$. Similarly, it computes $\underline{d}^j$, which contributes to the pure imaginary part of $\boldsymbol{d}^j$. Therefore, if we consider $J_{max}=3$, the desired output of this DT–CWT is

$$\begin{aligned}&\left[\bar{d}^1,\bar{d}^2,\bar{d}^3;\underline{d}^1,\underline{d}^2,\underline{d}^3\right]\\&\quad=\left[\Re\{\boldsymbol{d}^1\},\Re\{\boldsymbol{d}^2\},\Re\{\boldsymbol{d}^3\};\Im\{\boldsymbol{d}^1\},\Im\{\boldsymbol{d}^2\},\Im\{\boldsymbol{d}^3\}\right].\end{aligned}$$

The usual output is also the complex scale coefficients $\boldsymbol{c}^{J_{max}}$, which are not used in this method. In each scale decomposition j, the number of points on the time series is reduced by a factor of 2.

Therefore, the magnitude and the phase of the complex wavelet coefficients $\boldsymbol{d}^j$ for each scale j are given by

$$|\boldsymbol{d}^j|=\sqrt{|\Re(\boldsymbol{d}^j)|^2+|\Im(\boldsymbol{d}^j)|^2},\quad \angle\boldsymbol{d}^j=\phi^j=\arctan\left(\frac{\Im(\boldsymbol{d}^j)}{\Re(\boldsymbol{d}^j)}\right).$$

The $\underline{\psi}(t)$ is close to the Hilbert pair of $\bar{\psi}(t)$. In other words, $\underline{\psi}(t)\approx\mathcal{H}\{\bar{\psi}(t)\}$, where $\mathcal{H}$ denotes the Hilbert transform.[51–53]

In Ref. 45, it is shown that the implementation of the DT–CWT requires the first scale of the dual-tree filter bank to be different from the succeeding scales. In this work, we chose the Q-Shift (14, 14) tap-filters where scales $j>1$, which has provided a group delay of either 1/4 or 3/4 of a sample period and also satisfy the usual 2-band filterbank constraints of no aliasing and perfect reconstruction.[56] For the first scale, (13, 19) tap-filters were used, which are biorthogonal and near symmetric. The values for these filters are presented in Appendix B.

TABLE I. Non-zero near-symmetric (13, 19) and Q-shift (14, 14)—tap filter coefficients. Adapted from Ref. 53. The coefficients are multiplied by 10^{-2}.

			Q-shift			
	Near-symmetric		Upper tree		Lower tree	
n	$h_0^\star$	$h_1^\star$	$\bar{h}_0$	$\bar{h}_1$	$\underline{h}_0$	$\underline{h}_1$
1	−0.17578	-7.0626×10^{-5}	0.32531	−0.45569	−0.45569	−0.32531
2	0	0	−0.38832	0.54395	−0.54395	−0.38832
3	2.22660	0.13419	3.46600	1.70250	1.70250	−3.46600
4	−4.68750	−0.18834	−3.88730	−2.38250	2.38250	−3.88730
5	−4.82420	−0.71568	−11.72000	−10.67100	−10.67100	11.72000
6	29.68800	2.38560	27.53000	−1.18660	1.18660	27.53000
7	55.54700	5.56430	75.61500	56.88100	56.88100	−75.61500
8	29.68800	−5.16880	56.88100	−75.61500	75.61500	56.88100
9	−4.82420	−29.9760	1.18660	27.53000	27.53000	−1.18660
10	−4.68750	55.9430	−10.67100	11.72000	−11.72000	−10.67100
11	2.22660	−29.9760	2.38250	−3.88730	−3.88730	−2.38250
12	0	−5.16880	1.70250	−3.46600	3.46600	1.70250
13	−0.17578	5.56430	−0.54395	−0.38832	−0.38832	0.54395
14		2.38560	−0.45569	−0.32531	0.32531	−0.45569
15		−0.71568				
16		−0.18834				
17		0.13419				
18		0				
19		-7.0626×10^{-5}				

In the following, we describe and discuss how to compute the associated energy levels and, after that, the phase of a chaotic system using our DCWA method.

APPENDIX B: DUAL-TREE FILTERS

The dual-tree filters have the following desirable properties: approximate half-sample delay property, perfect reconstruction, finite support, vanishing moments, and linear phase filters, as can be seen in Ref. 45. The two low-pass filters should satisfy a very simple property: one of them should be approximately a half-sample shift of the other, $\underline{h}_0(n) \approx \bar{h}_0(n-0.5)$, because $\underline{\psi}(t) \approx \mathcal{H}\{\bar{\psi}(t)\}$.[53] Furthermore, in Ref. 45, three methods for dual-tree filter design are described, which are linear-phase biorthogonal solution, Q-Shift solution, and common-factor solution.[45]

The implementation of the DT–CWT requires that the first scale of the dual-tree filter bank be different from the succeeding scales, as shown in Ref. 45. If the same filters are used for each scale, then the first several scales of the filter bank will not be approximately analytic, i.e., it is locally given by a convergent power series. For the first scale, the condition $\underline{h}_0(n) \approx \bar{h}_0(n-1)$ must be satisfied exactly by using the same set of filters in each of the two trees, being necessary only to translate one set of filters by one sample with respect to the other set in Ref. 45. Moreover, any set of perfect reconstruction filters can be used for the first scale. Table I presents the analysis filters coefficients used in this work.

[1]A. S. Pikovsky, M. G. Rosenblum, and J. Kurths, *Synchronization: A Universal Concept in Nonlinear Sciences* (Cambridge University Press, New York, 2003).
[2]E. Rosa, E. Ott, and M. H. Hess, "Transition to phase synchronization of chaos," Phys. Rev. Lett. **80**, 1642–1645 (1998).
[3]M. G. Rosenblum, A. S. Pikovsky, and J. Kurths, "Phase synchronization of chaotic oscillators," Phys. Rev. Lett. **76**, 1804–1807 (1996).
[4]M. G. Rosenblum, A. S. Pikovsky, and J. Kurths, "From phase to lag synchronization in coupled chaotic oscillators," Phys. Rev. Lett. **78**, 4193–4196 (1997).
[5]M. G. Rosenblum, A. S. Pikovsky, J. Kurths, C. Schäfer, and P. A. Tass, "Phase synchronization: From theory to data analysis," in *Handbook of Biological Physics* (Elsevier, Amsterdam, 2001), Vol. 4, pp. 279–321.
[6]M. G. Rosenblum, A. S. Pikovsky, J. Kurths, G. V. Osipov, I. Z. Kiss, and J. L. Hudson, "Locking-based frequency measurement and synchronization of chaotic oscillators with complex dynamics," Phys. Rev. Lett. **89**, 264102 (2002).
[7]J. Buck, "Synchronous rhythmic flashing of fireflies II," Q. Rev. Biol. **63**, 265–289 (1988).
[8]L. Glass, "Synchronization and rhythmic processes in physiology," Nature **410**, 277–284 (2001).
[9]C. Schäfer, M. G. Rosenblum, H. H. Abel, and J. Kurths, "Synchronization in the human cardiorespiratory system," Phys. Rev. E **60**, 857–870 (1999).
[10]S. H. Strogatz and I. Stewart, "Coupled oscillators and biological synchronization," Sci. Am. **269**, 102–109 (1993).
[11]S. H. Strogatz, "Spontaneous synchronization in nature," in *IEEE International Frequency Control Symposium* (1997), pp. 2–4.
[12]S. Boccaletti, J. Kurths, G. Osipov, D. L. Valladares, and C. S. Zhou, "The synchronization of chaotic systems," Phys. Rep. **366**, 1–101 (2002).
[13]J. F. Heagy, T. L. Carroll, and L. M. Pecora, "Synchronous chaos in coupled oscillator systems," Phys. Rev. E **50**, 1874–1885 (1994).
[14]E. E. N. Macau, C. Grebogi, and Y. C. Lai, "Active synchronization in nonhyperbolic hyperchaotic systems," Phys. Rev. E **65**, 027202 (2002).
[15]L. M. Pecora and T. L. Carroll, "Synchronization in chaotic systems," Phys. Rev. Lett. **64**, 821–824 (1990).
[16]A. S. Pikovsky, M. G. Rosenblum, and J. Kurths, "Synchronization in a population of globally coupled chaotic oscillators," Europhys. Lett. **34**, 165–170 (1996).
[17]M. C. Romano, M. Thiel, J. Kurths, I. Z. Kiss, and J. L. Hudson, "Detection of synchronization for non-phase-coherent and non-stationary data," Europhys. Lett. **71**, 466 (2005).
[18]J. Kurths, M. C. Romano, M. Thiel, G. V. Osipov, M. V. Ivanchenko, I. Kiss, and J. L. Hudson, "Synchronization analysis of coupled noncoherent oscillators," Nonlinear Dyn. **44**, 135–149 (2006).

[19]T. Pereira, M. S. Baptista, and J. Kurths, "General framework for phase synchronization through localized sets," Phys. Rev. E **75**, 026216 (2007).
[20]R. Follmann, E. E. N. Macau, and E. Rosa, "Detecting phase synchronization between coupled non-phase-coherent oscillators," Phys. Lett. A **373**, 2146–2153 (2009).
[21]R. Follmann, E. E. N. Macau, and E. Rosa, "Phase detection of chaos," Phys. Rev. E **83**, 016209 (2011).
[22]I. Daubechies, J. Lu, and H. T. Wu, "Synchrosqueezed wavelet transforms: An empirical mode decomposition-like tool," Appl. Comput. Harmonic Anal. **30**, 243–261 (2011).
[23]B. Kralemann, M. Frühwirth, A. Pikovsky, M. Rosenblum, T. Kenner, J. Schaefer, and M. Moser, "*In vivo* cardiac phase response curve elucidates human respiratory heart rate variability," Nat. Commun. **4**, 2418 (2013).
[24]M. G. Rosenblum and J. Kurths, "Analysing synchronization phenomena from bivariate data by means of the Hilbert transform," in *Nonlinear Analysis of Physiological Data* (Springer, 1998) pp. 91–99.
[25]A. E. Hramov and A. A. Koronovskii, "An approach to chaotic synchronization," Chaos **14**, 603–610 (2004).
[26]A. E. Hramov, A. A. Koronovskii, and Y. Levin, "Synchronization of chaotic oscillator time scales," J. Exp. Theor. Phys. **100**, 784–794 (2005).
[27]A. E. Hramov, A. A. Koronovskii, V. I. Ponomarenko, and M. D. Prokhorov, "Detection of synchronization from univariate data using wavelet transform," Phys. Rev. E **75**, 056207 (2007).
[28]A. A. Koronovskii and A. E. Hramov, "Chaotic phase synchronization studied by means of continuous wavelet transform," Tech. Phys. Lett. **30**, 587–590 (2004).
[29]A. A. Koronovskii and A. E. Hramov, "Wavelet transform analysis of the chaotic synchronization of dynamical systems," JETP Lett. **79**, 316–319 (2004).
[30]A. A. Koronovskii, M. Kurovskaya, and A. E. Hramov, "Relationship between phase synchronization of chaotic oscillators and time scale synchronization," Tech. Phys. Lett. **31**, 847–850 (2005).
[31]A. A. Koronovskii, V. I. Ponomarenko, M. D. Prokhorov, and A. E. Hramov, "Diagnostics of the synchronization of self-oscillatory systems by an external force with varying frequency with the use of wavelet analysis," J. Commun. Technol. Electron. **52**, 544–554 (2007).
[32]E. B. Postnikov, "On precision of wavelet phase synchronization of chaotic systems," J. Exp. Theor. Phys. **105**, 652–654 (2007).
[33]E. B. Postnikov, "Wavelet phase synchronization and chaoticity," Phys. Rev. E **80**, 057201 (2009).
[34]L. W. Sheppard, A. Stefanovska, and P. V. E. McClintock, "Testing for time-localized coherence in bivariate data," Phys. Rev. E **85**, 046205 (2012).
[35]A. V. Tankanag, A. A. Grinevich, T. V. Kirilina, G. V. Krasnikov, G. M. Piskunova, and N. K. Chemeris, "Wavelet phase coherence analysis of the skin blood flow oscillations in human," Microvasc. Res. **95**, 53–59 (2014).
[36]A. E. Hramov and A. A. Koronovskii, "Time scale synchronization of chaotic oscillators," Physica D **206**, 252–264 (2005).
[37]R. Q. Quiroga, A. Kraskov, T. Kreuz, and P. Grassberger, "Performance of different synchronization measures in real data: A case study on electroencephalographic signals," Phys. Rev. E **65**, 041903 (2002).
[38]M. L. V. Quyen, J. Foucher, J. P. Lachaux, E. Rodriguez, A. Lutz, J. Martinerie, and F. J. Varela, "Comparison of Hilbert transform and wavelet methods for the analysis of neuronal synchrony," J. Neurosci. Methods **111**, 83–98 (2001).
[39]M. T. Ferreira, C. B. N. Freitas, M. O. Domingues, and E. E. N. Macau, "The discrete complex wavelet approach to phase assignment and a new test bed for related methods," Chaos **25**, 013117 (2015).
[40]M. T. Ferreira, R. Follmann, M. O. Domingues, and E. E. N. Macau, "Detecting phase synchronization in coupled chaotic non-coherent oscillators by using complex wavelet transform," in *11th International Conference on Vibration Problems - ICOVP* (2013), pp. 1–8.
[41]M. T. Ferreira, M. O. Domingues, and E. E. N. Macau, "Detecting phase synchronization in chaotic non-coherent Rössler systems using discrete complex wavelet approach (DCWA): preliminaries results," in *Proceeding Series of the Brazilian Society of Computational and Applied Mathematics* (2016), Vol. **4**, pp. 010047–1–010047–7.
[42]M. T. Ferreira, R. Follmann, M. O. Domingues, and E. E. N. Macau, "Aplicação da transformada wavelet complexa dual-tree na detecção de sincronização de fase entre sistemas caóticos de Lorenz," in *Anais do Congresso de Matemática Aplicada e Computacional - CMAC Sudeste* (2013), pp. 414–419.
[43]M. T. Ferreira, M. O. Domingues, and E. E. Macau, "Phase synchronization based on a dual-tree complex wavelet transform," EPJST **225**, 2679–2688 (2016).
[44]M. T. Ferreira, C. B. N. Freitas, M. O. Domingues, and E. E. N. Macau, "Modelo de Kuramoto e a verificação da diferençe fase usando uma metodologia baseada na transformada wavelet complexa dual-tree: Resultados preliminares," in *Proceeding Series of the Brazilian Society of Applied and Computational Mathematics* (2013), Vol. **1**, pp. 010127–1–010127–4.
[45]I. W. Selesnick, R. G. Baraniuk, and N. G. Kingsbury, "The dual-tree complex wavelet transform," IEEE Signal Proc. Mag. **22**, 123–151 (2005).
[46]J. Y. Chen, K. W. Wong, and J. W. Shuai, "Properties of phase locking with weak phase-coherent attractors," Phys. Lett. A **285**, 312–318 (2001).
[47]O. E. Rössler, "An equation for continuous chaos," Phys. Lett. A **57**, 397–398 (1976).
[48]M. Wickramasinghe and I. Z. Kiss, "Phase synchronization of three locally coupled chaotic electrochemical oscillators: Enhanced phase diffusion and identification of indirect coupling," Phys. Rev. E **83**, 016210 (2011).
[49]J. Nawrath, M. C. Romano, M. Thiel, I. Z. Kiss, M. Wickramasinghe, J. Timmer, J. Kurths, and B. Schelter, "Distinguishing direct from indirect interactions in oscillatory networks with multiple time scales," Phys. Rev. Lett. **104**, 038701 (2010).
[50]N. G. Kingsbury, "The dual-tree complex wavelet transform: A new efficient tool for image restoration and enhancement," in *Signal Processing Conference (EUSIPCO)* (IEEE, 1998), pp. 319–322.
[51]N. G. Kingsbury, "Shift invariant properties of the dual-tree complex wavelet transform," in *IEEE International Conference on Acoustics, Speech, and Signal Processing (ICASSP)* (IEEE, 1999), pp. 1221–1224.
[52]N. G. Kingsbury, "A dual-tree complex wavelet transform with improved orthogonality and symmetry properties," in *Proceedings of IEEE International Conference on Image Processing* (IEEE, 2000), Vol. **2**, pp. 375–378.
[53]N. G. Kingsbury, "Complex wavelets for shift invariant analysis and filtering of signals," J. Appl. Comput. Harmonic Anal. **10**, 234–253 (2001).
[54]I. Daubechies, "The wavelet transform, time-frequency localization and signal analysis," IEEE Trans. Inf. Theory **36**, 961–1005 (1990).
[55]S. G. Mallat, *A Wavelet Tour of Signal Processing* (Academic Press, New York, 1998).
[56]N. Kingsbury, "Design of q-shift complex wavelets for image processing using frequency domain energy minimization," in *Proceedings of IEEE International Conference on Image Processing* (IEEE, 2003), Vol. **1**, pp. 1013–1016.